

## **Repercussions of available long offset, random noise and impedance contrast on AVO analysis**

Sergio Romahn and Kris Innanen

### **ABSTRACT**

The amplitude variation with offset (AVO) or angle of incidence (AVA) is sensible to several factors that may affect the feasibility of doing this kind of analysis. This work evaluates how the available long offset, level of random noise and impedance contrast affect the estimation of the AVO parameters (intercept, gradient and curvature). An oil sand, with a class-III AVO anomaly, constitutes the geological framework. Fluid replacement modelling was used in order to extend the analysis to three different impedance contrast scenarios: gas, oil and water filling the pore space. Firstly, we analyzed the AVO response with no noise and offsets related to angle of incidence up to 45 degrees. This case was taken as reference to measure the error and standard deviation in the AVO-parameter estimation when decreasing the available offset and varying the level of noise. The results, for the gas case, show that the intercept is practically not impacted by the reduction of offset and is slightly affected by the level of noise. Errors around 3% were obtained with angle traces up to 15 degrees and S/N equals 2. The gradient is strongly affected by the maximum available offset and signal to noise ratio. Errors smaller than 20% allow estimating meaningful values of the gradient. 20% of error can be obtained with several combinations of maximum angle and level of noise, for example: angle traces up to 45 degrees and low S/N of 3, or angle traces up to 22 degrees and high S/N of 15. The most affected parameter is the curvature. We would need angle traces greater than 36 degrees and high S/N of 15 to produce errors smaller than 20%. If the  $S/N \leq 5$  we would need angles traces of 45 degrees to abstain the same error. When comparing the gas, oil and water scenarios, we observe that the error increases as the impedance contrast decreases. These results may be relevant when designing a seismic survey or for time-lapse seismic purposes.

### **INTRODUCTION**

The maximum distance between source and receiver (offset) is a relevant parameter when designing a seismic survey. Cordson et-al (2000) state that the maximum offset depends on the depth of the deeper targets to be imaged, and they emphasize, along with Galbraith (2004), on the impact of the processing mute. This work introduces another criterion that can be used when designing a seismic survey: recording the maximum offset needed to perform AVO analysis. On the other hand, random noise also affects AVO response. Downton and Lines (2001) studied the impact of random noise in AVO inversion and proposed a methodology to know the feasibility of applying this technique in the presence of noise. Cambois (1998) recognized that noise can lead to misinterpretation of the background shale trend when applying AVO attributes such as fluid factor. We analyzed the simultaneous effect of maximum offset and level of noise in AVO analysis, specifically on the estimation of intercept, gradient and curvature parameters. We also addressed how the AVO response changes as the impedance contrast decreases.

We used the following information for this experiment: density, P- and S-wave velocity logs (Fig. 1). The original logs correspond to oil filling the pore space. The 30-m thick reservoir, from 1.844 to 1.867 s, is characterized by a P-wave interval velocity of 2690 m/s, S-wave interval velocity of 1680 m/s and density of 2.1 g/cc. The seal constituted by a shale layer has P-wave interval velocity, S-wave interval velocity and density of 3200 m/s, 1600 m/s and 2.33 g/cc, respectively.

The method of analysis is as follows: Firstly, fluid replacement modelling, based on Gassmann theory (Gassmann, 1951; Smith et-al, 2003), was used to generate new velocity and density logs by substituting the original fluid (oil) by gas and water, while holding all other rock parameters (matrix composition, porosity, thickness) constant.

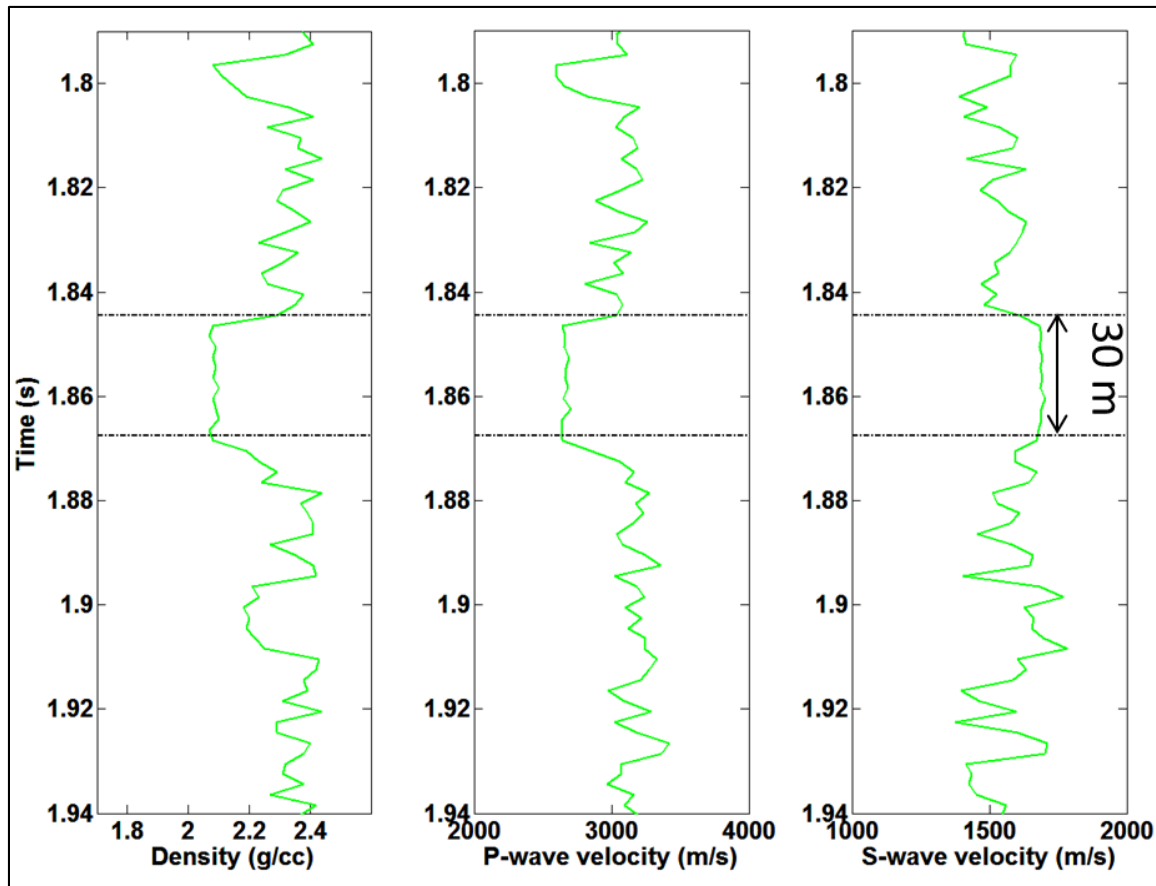


FIG. 1. Log data of an oil-producing well. Density, P- and S-wave velocity logs are required for this experiment.

Secondly, seismic gathers were generated by modelling amplitude variation with angle of incidence, applying the Zoeppritz equations and the convolutional model of the Earth. Angles of incidence were directly used instead of offset for the modelling process.

The third step was to apply the Wiggins reformulation of the Aki-Richards (2002) approximation as used by Russell and Hampson (2006) to estimate the intercept, gradient and curvature for each time of the synthetic gather:

$$R_P(\theta) = R_{AI} + G \sin^2 \theta + R_{VP} \sin^2 \theta \tan^2 \theta \quad (1)$$

Where the first term is the intercept

$$R_{AI} = \frac{1}{2} \left[ \frac{\Delta V_P}{\overline{V_P}} + \frac{\Delta \rho}{\overline{\rho}} \right]$$

G in the second term is the gradient

$$G = \frac{\Delta V_P}{2\overline{V_P}} - \frac{4}{\gamma^2} \frac{\Delta V_S}{\overline{V_S}} - \frac{2}{\gamma^2} \frac{\Delta \rho}{\overline{\rho}}$$

$$\gamma = \frac{V_S}{V_P}$$

And  $R_{VP}$  is the curvature

$$R_{VP} = \frac{\Delta V_P}{2\overline{V_P}}$$

An important assumption is that equation 1 fits the amplitude versus angle curve.

The AVO parameters, derived from a gather with no noise and angles up to 45 degrees, were taken as reference to measure the error when reducing angle of incidence and varying the signal to noise ratio.

Because of the random nature of noise, the experiment was repeated several times for each level of noise and maximum available angle, in such way that we can calculate the relative error and the standard deviation which is representative of the dispersion degree of the estimations.

Finally, the standard deviation as a function of angle and noise was plotted for gas, oil and water scenarios. These kind of plots allow comparing the effect of different impedance contrasts in AVO analysis, and can be used for deciding the maximum offset when designing a seismic survey.

### **LABORATORY PROCEDURE AND DATA ANALYSIS**

The new velocity logs (gas and water cases), obtained by applying fluid substitution, and the original logs, corresponding to oil filling the pore space, are displayed in Fig. 2. Gas produces a significant decrement of P-wave velocity and density, and a subtle increase in S-wave velocity. Water produces the opposite change: P-wave velocity and density rise, while S-wave velocity slightly falls.

Considering the P-wave velocity for each fluid scenario and the reservoir's thickness of 30 m, we would need dominant frequencies of 21, 22 and 24 Hz to resolve the gas, oil and water cases, respectively (Table 1). By using a zero-phase Ricker wavelet with a dominant frequency of 25 Hz, we properly resolve the sand of interest for the three fluid scenarios. The top and the base of the reservoir approximately coincide with the maximum negative and maximum positive amplitudes, respectively.

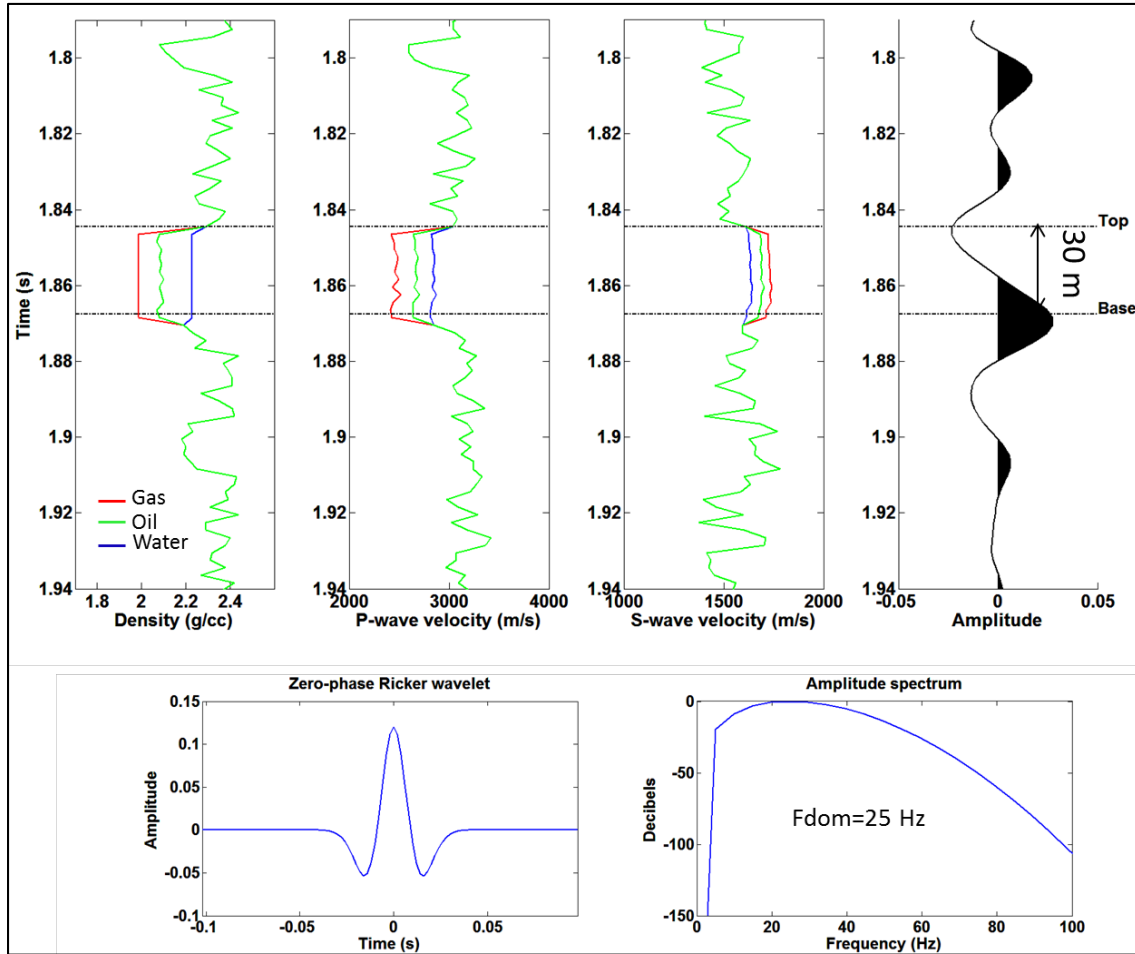


FIG. 2. Well log data of an oil-producing well. The original logs with oil filling the pore space are in green. The red and blue lines correspond to gas and water, respectively. A zero-phase Ricker wavelet with dominant frequency of 25 Hz properly resolves the reservoir.

Table 1. Dominant frequency needed to resolve a 30-m thick target using the quarter wavelength criterion.

	Thickness (m)	30
	P-wave vel (m/s)	Fdom (Hz)
GAS	2500	21
OIL	2690	22
WAT	2850	24

Fig. 3 shows the variation of the PP-reflection coefficient with angle calculated by using the Zoeppritz equations. Gas, oil and water cases are compared in this plot. Gas produces the higher reflection coefficient and larger changes in amplitude with angle, followed by the oil case. Water generates smaller reflection coefficients and subtle changes of amplitude with angles below 50 degrees. We observe that the critical angle decreases as the impedance contrast increases. We used pre-critical angles up to 45 degrees for this experiment.

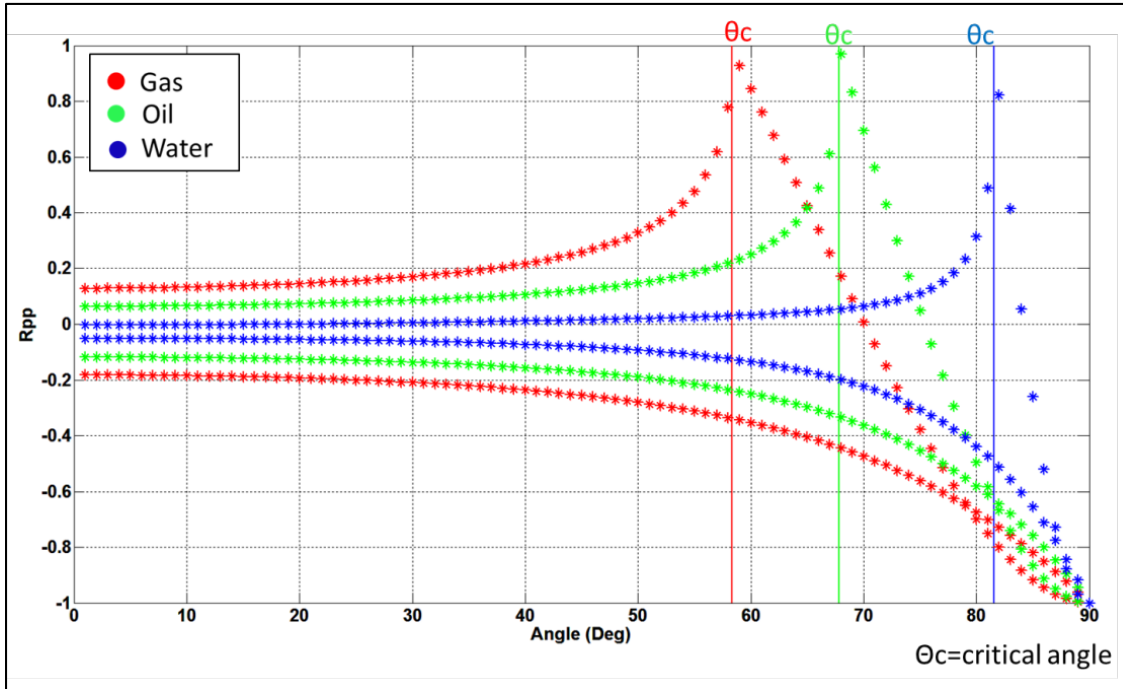


FIG. 3. PP-reflection coefficient variation with angle for gas, oil and water scenarios.

Fig. 4 shows the synthetic seismic gathers constructed by using the wavelet and well-logs in Fig. 2 and applying Zoeppritz equations. No noise was introduced in this case. The top and base of the sand of interest are highlighted at 1844 and 1867 ms, respectively. The gathers are constituted by angle traces from 1 to 45 degrees. The relationship between angle and offset is shown in Fig. 5. Large angles mean large offsets as described by the approximation:

$$\sin \theta = \frac{X V_{int}}{t V_{rms}^2} \quad (2)$$

Where  $\theta$  is angle of incidence,  $X$  is offset,  $t$  is total traveltime,  $V_{int}$  is interval velocity, and  $V_{rms}$  is root mean square velocity.

By comparing the synthetic gathers, we observe that gas originates the largest impedance contrast; thus, higher amplitudes are produced for this case. On the other hand, when we have water in the pore space, there is a weak impedance contrast between the sand and the surrounding shale; therefore, a weak reflection is generated.

The amplitude variation with angle for the top and base of the three fluid scenarios are shown in the bottom left corner of Fig. 4. When water fills the pore space, traces that are close to zero degrees have an amplitude significantly smaller compared to the gas and oil cases, and there is no significant amplitude variation with angle. On the other hand, there is a relevant amplitude increment with angle for the gas and oil cases, the gas case being the one showing the greatest amplitude variation.

The intercept and gradient parameters derived by fitting equation 1 to the amplitude vs angle points are shown in the bottom right corner of Fig. 4. We observe that the intercept vs gradient plot is able to discriminate fluids. Points related to shale and sands with water

are concentrated in a zone that is called “background”, while the points of the gas and oil sand are well separated from the background. The gas points tend to be more separated from the background because of the high impedance contrast and large amplitude variation with angle. The intercept, gradient and curvature parameters for gas, oil and water are shown in Table 2. These values were taken as reference to measure the error when decreasing the maximum angle and varying the level of noise.

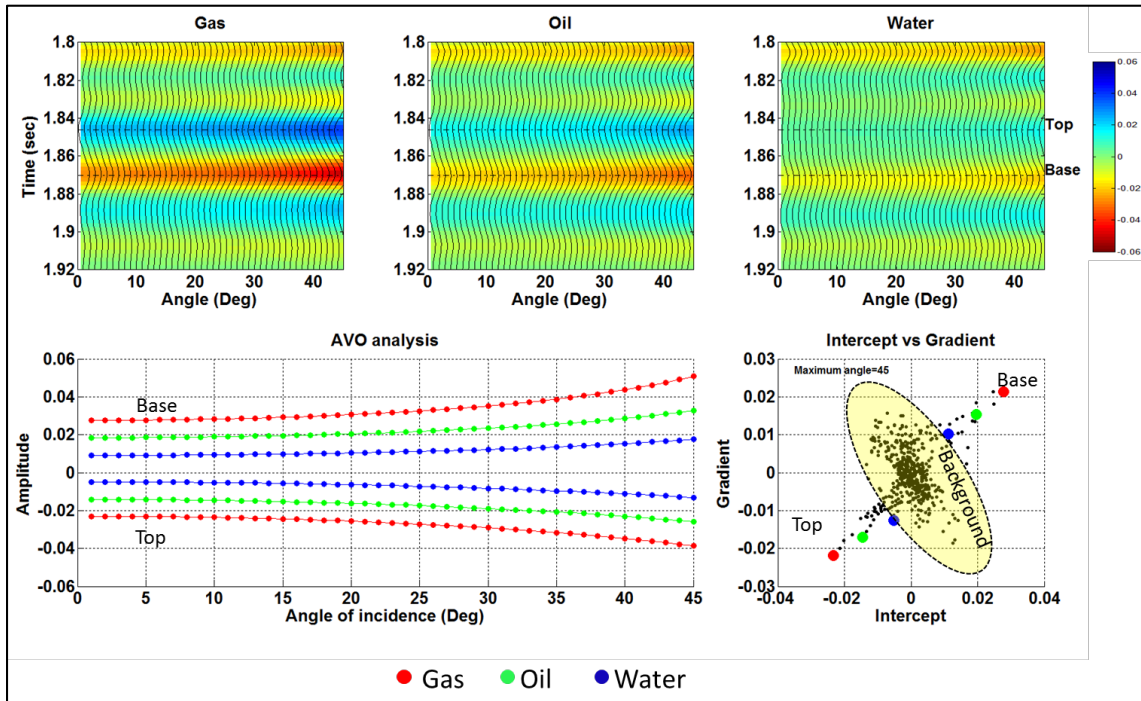


FIG. 4. AVO modelling and analysis of the AVO response applied to gas, oil and water scenarios.

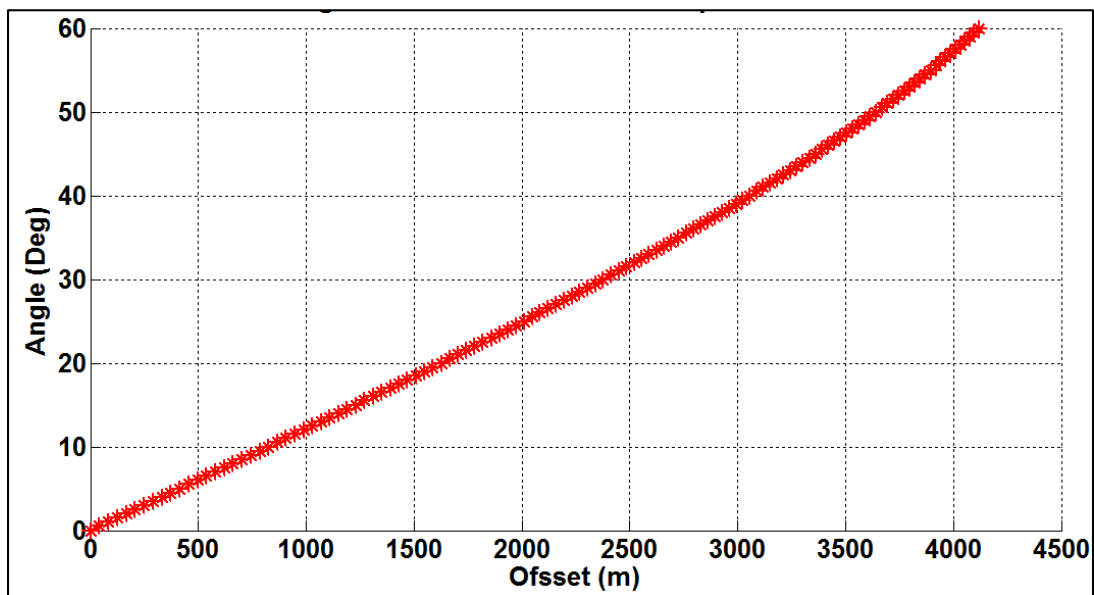


FIG. 5. Relationship between angle of incidence and offset at the top of the reservoir

Table 2. AVO parameters estimated from synthetic gathers with no noise and using angle traces up to 45 degrees.

	TOP			BASE		
	Intercept	Gradient	Curvature	Intercept	Gradient	Curvature
<b>GAS</b>	-0.023	-0.021	-0.010	0.028	0.022	0.024
<b>OIL</b>	-0.014	-0.017	-0.007	0.018	0.016	0.013
<b>WATER</b>	-0.005	-0.012	-0.004	0.009	0.010	0.007

### Effect of random noise on AVO-parameter estimation

Several signal-to-noise ratios were tested to see the impact of random noise on AVO response while keeping constant the angle range from 1 to 45 degrees. Fig. 6 shows the amplitude variation with angle and the intercept vs gradient plots for the three fluid scenarios using S/N equals 2, 4, 6, 8, 10 and 12. We observe some stability on the parameter estimation with S/N above 6. Based on one observation only, we could say that the results when S/N equals 4 and 2 are acceptable. However, we are not able to perceive the actual impact of noise with only one observation because of the random nature of the noise. In order to know the impact of the noise, we estimated the AVO-parameters several times and measured the dispersion of the estimations statistically.

### Error and dispersion measurement

The relative error of the AVO-parameter was calculated by using:

$$e_{rel} = \frac{P - P_{ref}}{P_{ref}} \quad (3)$$

Where P is the intercept, gradient or curvature values estimated with a particular S/N and angle range, and  $P_{ref}$  is the AVO parameter measure with no noise and using angles from 1 to 45 degrees (Table 2). Given that AVO-parameters were estimated for the top and base of the reservoir, the total relative error is an average of the error derived from these two events.

We repeated the parameter estimation 100 times for each S/N and angle range, so that we have 100 measurements of the error. From these errors we calculate the mean relative error and the standard deviation. Fig. 7 graphically shows this procedure for an angle range from 1 to 45 and S/N equals 2.

The standard deviation measures the dispersion and provides information about the quality of the AVO-parameter estimation. Given that the mean relative error fluctuates around zero, the standard deviation becomes the best representation of the maximum error.

Fig. 8 shows the dispersive effect of noise on intercept versus gradient crossplots for different levels of noise, while keeping constant the maximum angle of 45 degrees. 100 measurements were taken for each level of noise, thus allowing noticing its actual impact. We observe that the dispersion of the parameter estimation decreases as the S/N increases. Random noise slightly impacts the intercept. Conversely, the gradient is strongly affected, specially with S/N under 4.

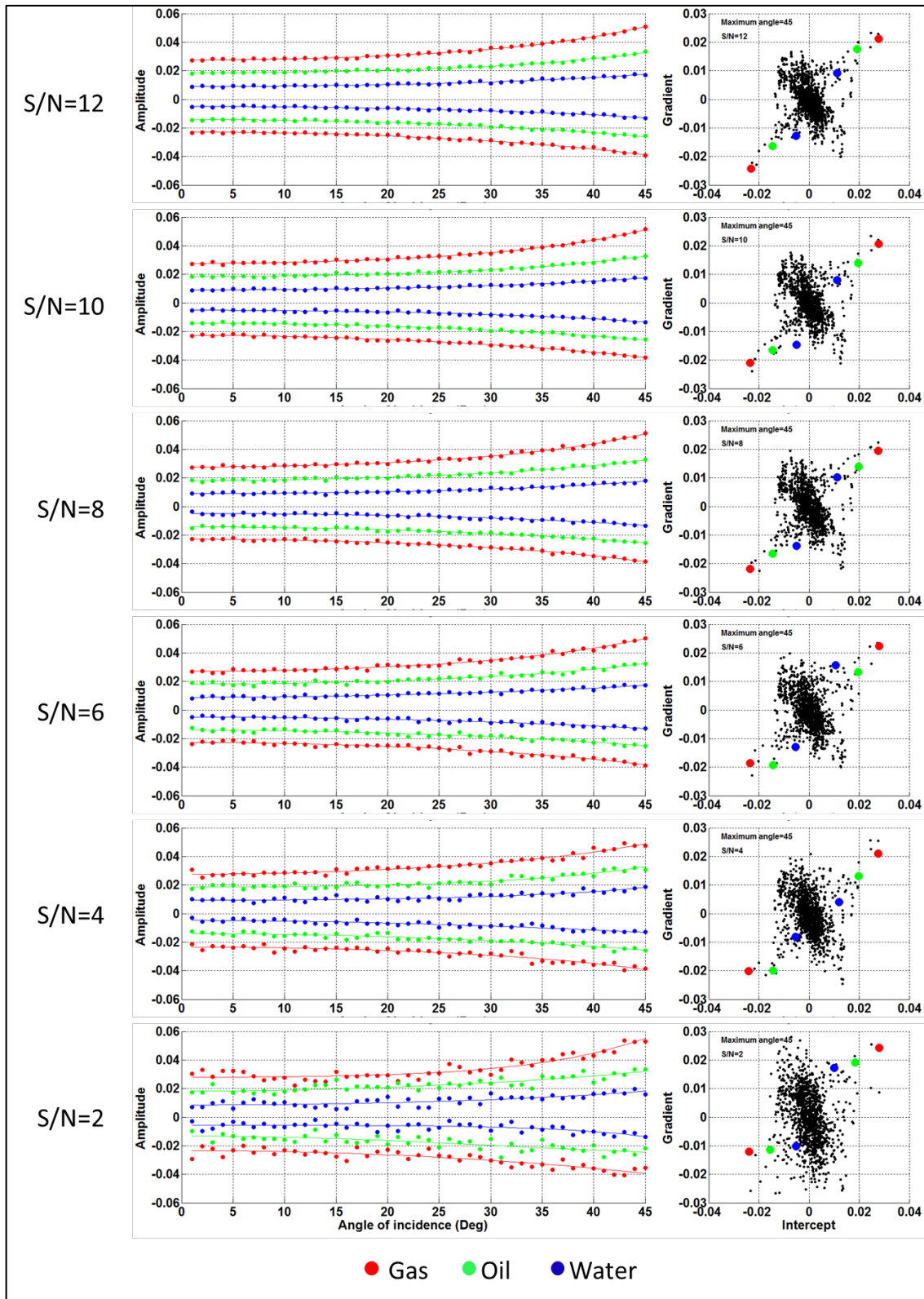


FIG. 6. Effect of random noise on AVO response.

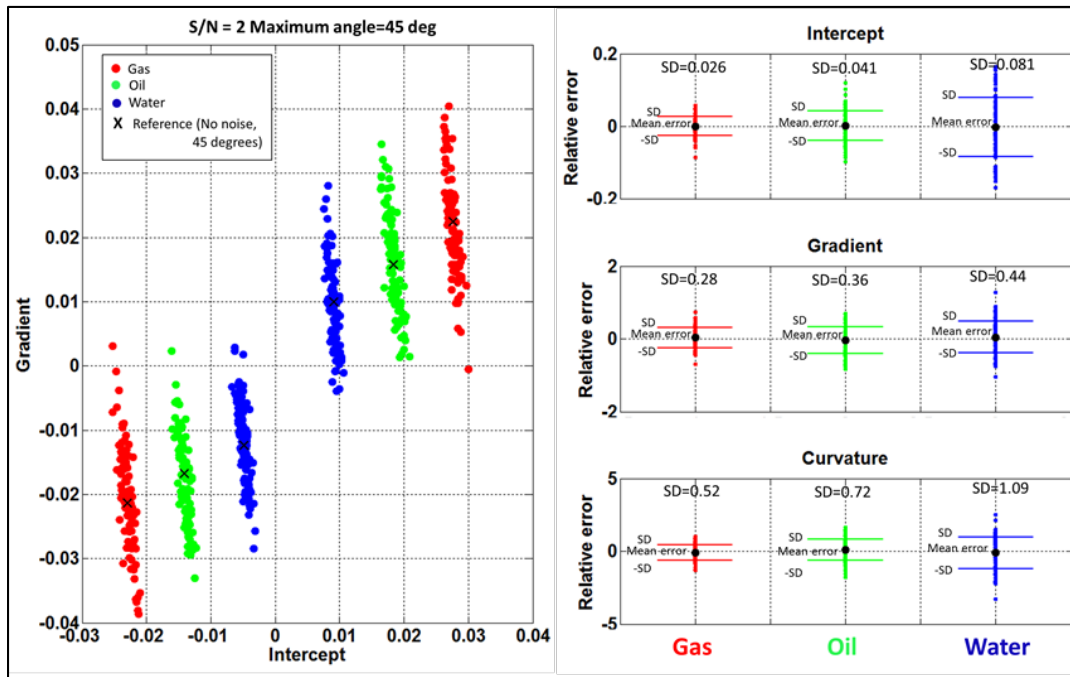


FIG. 7. AVO-parameter dispersion because of random noise. The standard deviation effectively describes the dispersion.

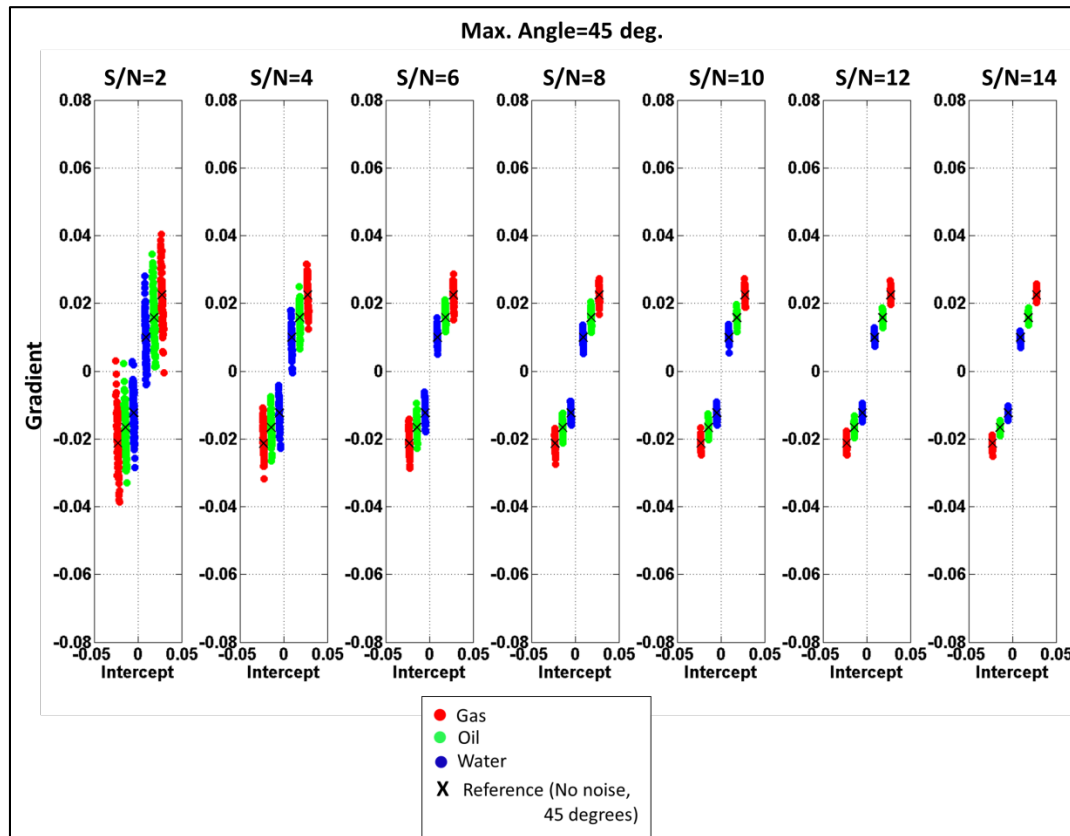


FIG.8 Effect of varying level of noise on intercept vs gradient plot. The maximum angle of 45 degrees was kept constant.

Fig. 9 shows the relative error and the standard deviation for gas, oil and water scenarios when varying S/N and keeping the angle range from 1 to 45 degrees. The mean relative error calculated from 100 measurements does not reflect how the AVO response deteriorates as S/N is reduced. On the other hand, the standard deviation properly represents the effect of increasing noise. We observe that the standard deviation increases as we go from gas to oil, and finally water. This suggests that the error when estimating AVO parameters increases as the impedance contrast decreases.

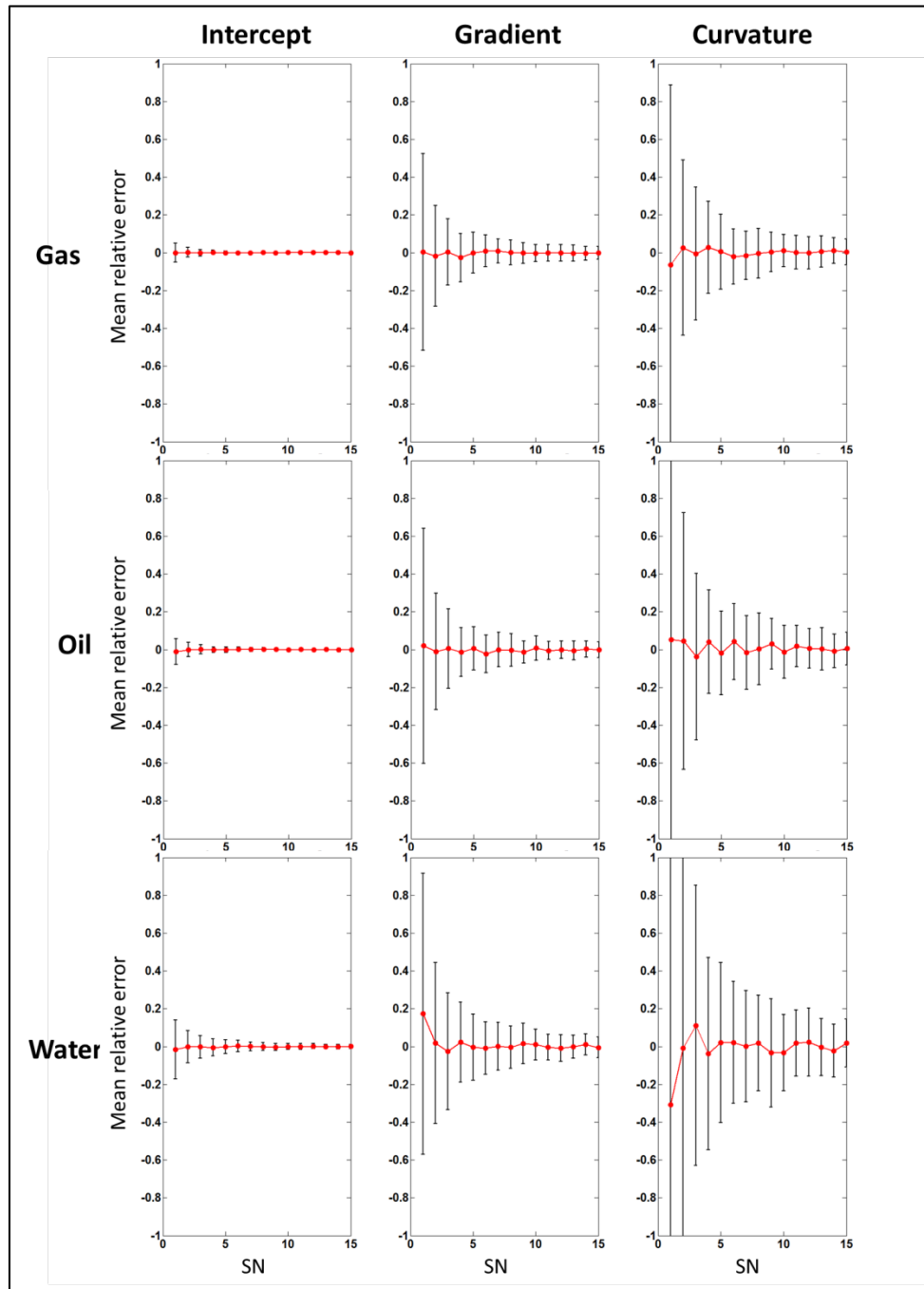


FIG. 9. Effect of varying S/N. Mean relative error and standard deviation for gas, oil and water scenarios.

## Effect of reducing maximum available offset (angle of incidence) on AVO-parameter estimation

The impact of reducing the angle of incidence on the intercept vs gradient plot is shown in Fig. 10. A signal to noise ratio of 12 was kept constant. The first panel corresponds to the angle range from 1 to 15 degrees. We subsequently increased 5 angles up to a 45-degree angle trace. We observe that the dispersion of the AVO-parameters decreases as we use more angle traces. A relevant improvement is observed when we go from 20 to 25 degrees. After that, the dispersion is gradually reduced.

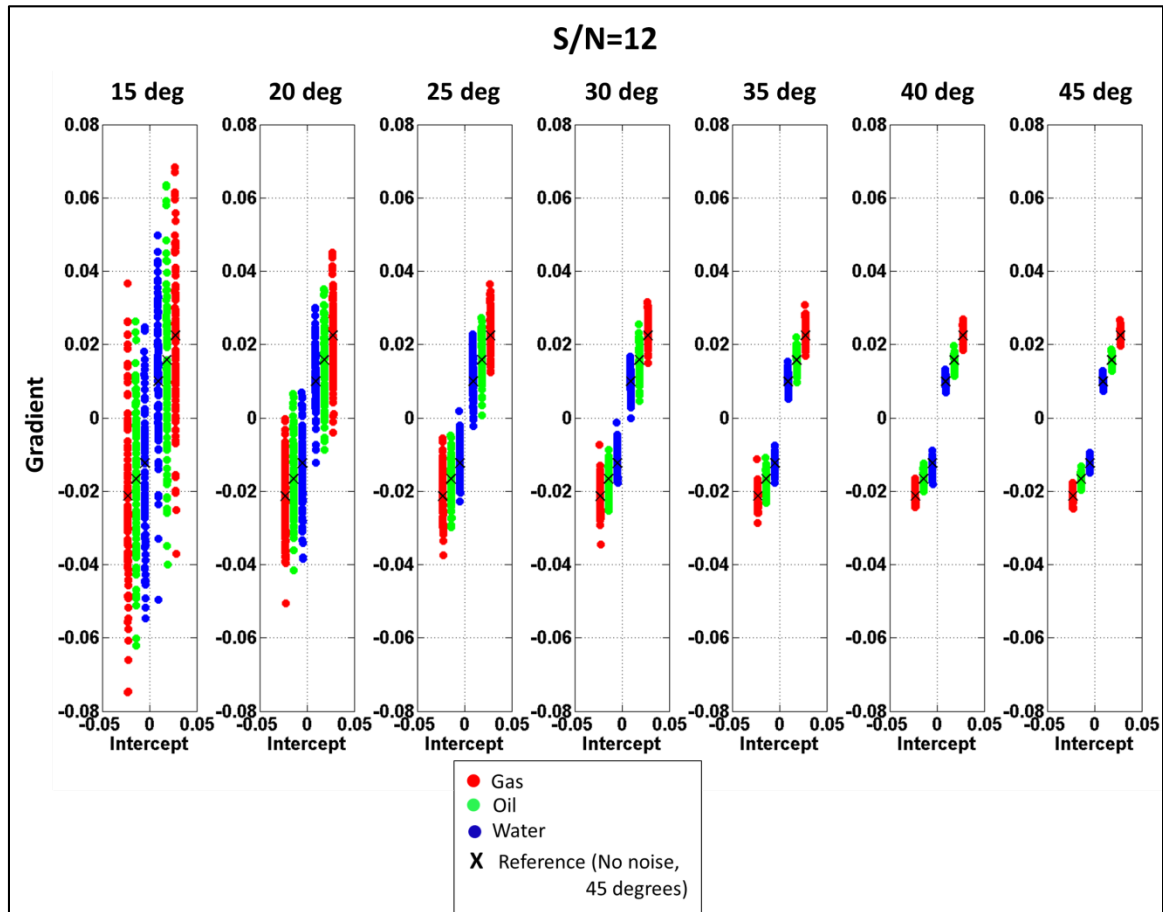


FIG. 10. Effect of reducing angle of incidence on intercept vs gradient plot. S/N=12 was kept constant.

Fig. 11 shows the relative error and the standard deviation for gas, oil and water scenarios when reducing the maximum angle and keeping S/N=12. The standard deviation denotes how the estimation of the AVO-parameters improves as we add more angle traces. We observe that AVO-parameter estimation is stable when the error is smaller than 20%.

For the gas case, the intercept does not have a significant error because it depends on small angle traces. The maximum error with traces up to 15 degrees would be 0.6%. The gradient can be estimated with errors smaller than 20% if we have angle traces greater than 22 degrees. The curvature is the most sensitive parameter to long offset information.

It can be estimated with errors smaller than 20% if we have angle traces greater than 36 degrees. We can see that the error increases as the impedance contrast decreases.

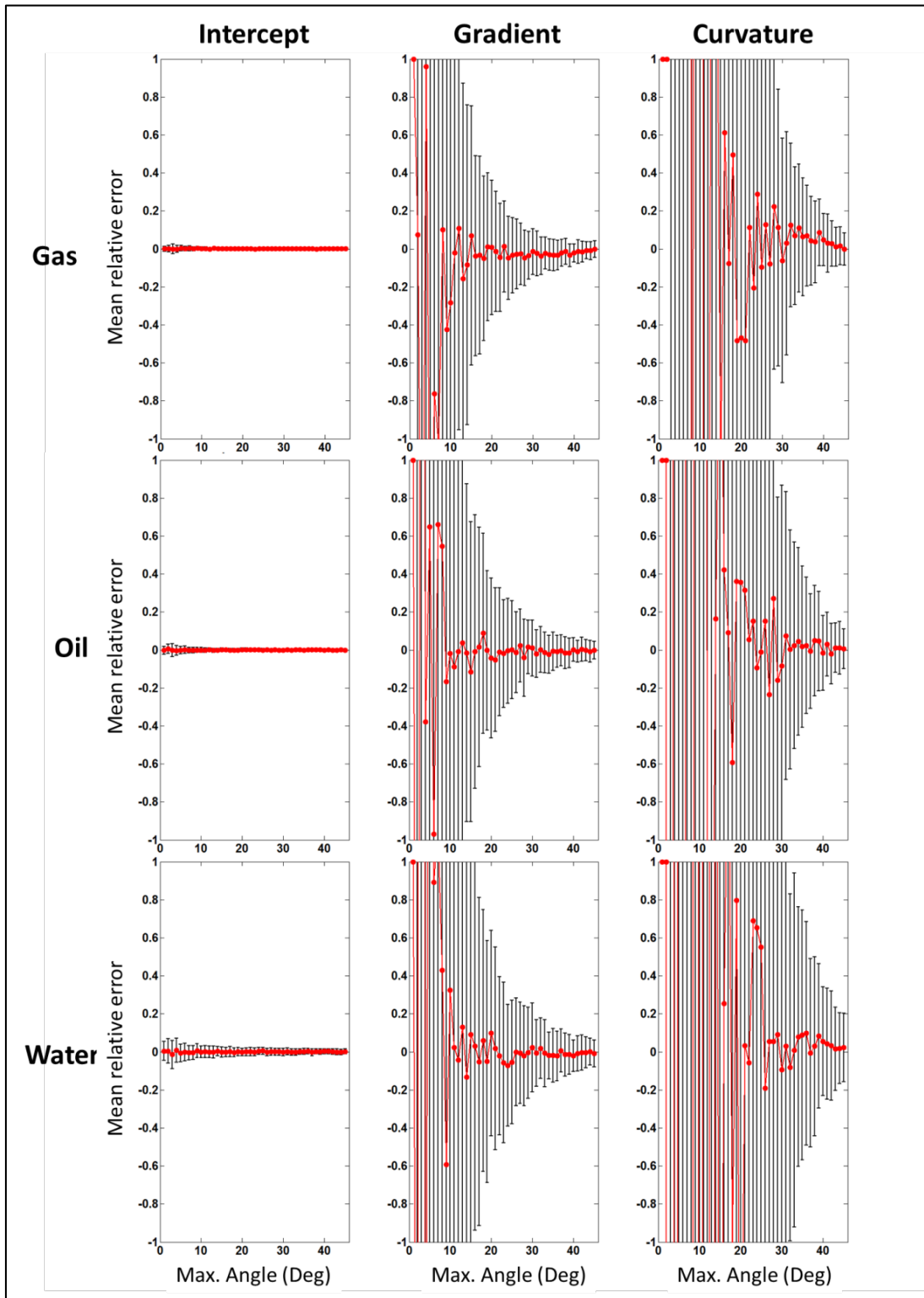


FIG. 11. Effect of reducing maximum angle of incidence. Mean relative error and standard deviation for gas, oil and water scenarios. S/N=12 was kept constant.

### Simultaneous effect of noise and maximum angle available

Fig. 12 shows the standard deviation matrix constructed by varying S/N from 1 to 15 and maximum angle available from 10 to 45 for the three AVO-parameters and the three fluid scenarios. An error cut-off of 20% was selected considering the instability of the parameter estimations with errors greater than that.

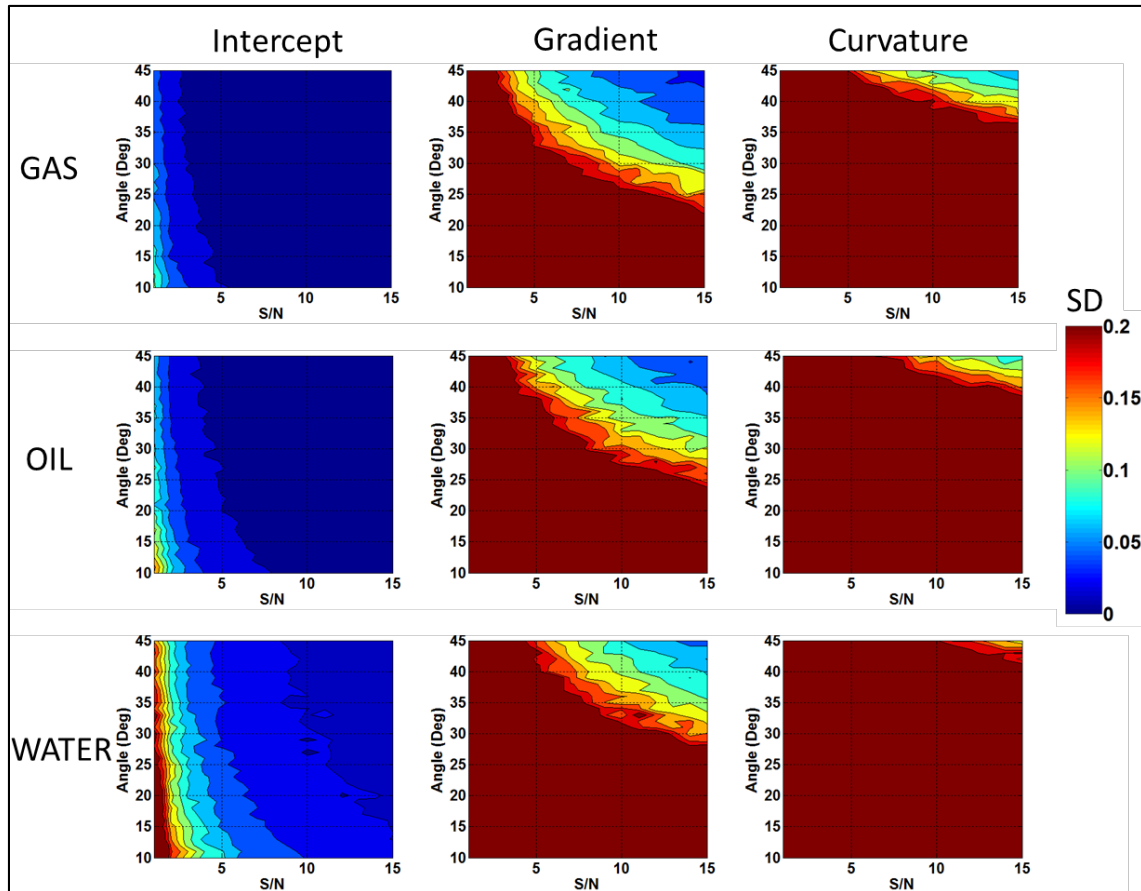


FIG. 12. Simultaneous effect of noise and maximum angle available on AVO-parameter estimation

These plots provide a criterion to decide the maximum offset when designing seismic surveys, taking into consideration a specific impedance contrast and the expected level of noise. For example, if we anticipate a  $S/N=5$  and an impedance contrast similar to the gas scenario, we would design a maximum angle of 35 degrees (offset=2750 m) and expect maximum errors below 20%. If we expect an impedance contrast such as the oil case, we would either need to acquire angles of 40 degrees (offset=3000 m) or to improve the  $S/N$  by processing so that we obtain similar errors (Fig. 13). If we design a seismic survey considering the higher impedance contrast, we are already covering scenarios with lower impedance contrast. Long offsets contribute to stabilize the estimation of the AVO-parameters. It is recommendable to acquire larger offsets when the expected  $S/N$  is lower than 4.

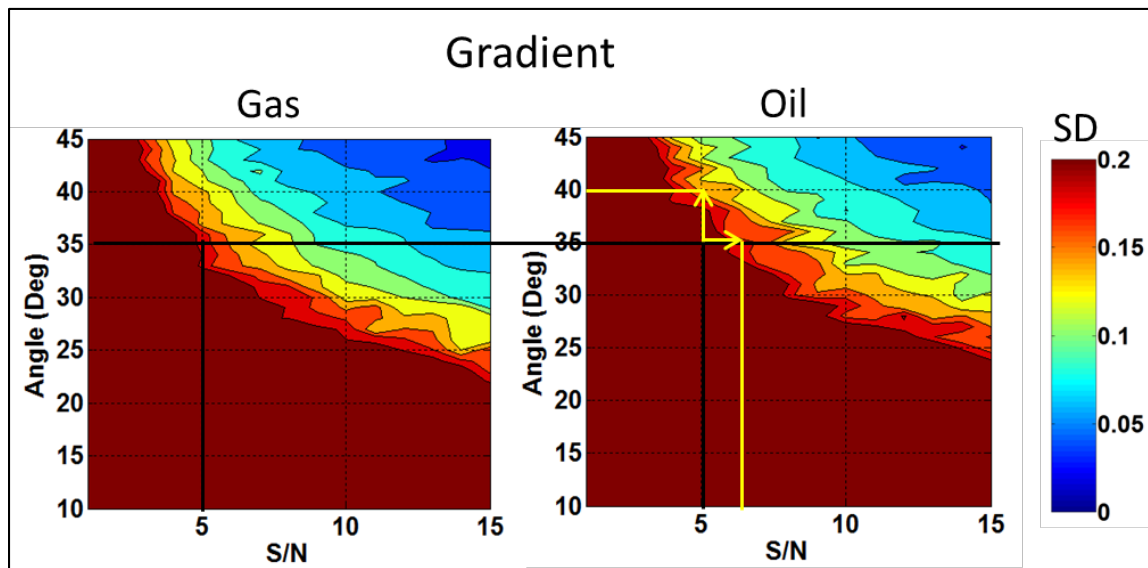


FIG. 13. Standard deviation matrix for gas and oil cases. These plots allow us to decide the maximum offset when designing a seismic survey.

## DISCUSSION

The synthetic seismic gathers in this work were generated directly by angles instead of offsets. We compared these angle gathers with the respective offset gathers converted to angle gathers using ray tracing, and no difference arose in the angle range of analysis. However, a more complete analysis may include gathers with raytracing modelling so that NMO stretching effect is included. A more complete experiment may incorporate multiples and transmission loss.

Normalized noise was produced by using “noise” from CREWES software. The level of noise is created based on the rms level of an input signal in a specific window of interest. For this experiment, the input signal was the seismic gather with no noise and the whole trace was taken to calculate the rms level. Different level of noise may arise if we consider other windows to calculate the rms level. We will test other distributions of noise in future experiments.

This experiment was conducted under the geological framework given by the well, which has a class-III AVO response. Although different geological settings will give place to different results, we can use this methodology for a better understanding of the AVO phenomenon. Future work will test the repercussions of random noise and maximum available offset in different geological frameworks.

## CONCLUSIONS

The lack of large offset information and random noise produces instability in the AVO-parameter estimation, particularly for the gradient and curvature. The instability is presented as a dispersion of the parameter after repeating several observations. This dispersion is significant when the error is greater than 20%. By plotting the error as a function of S/N and maximum available angle and applying a cut-off of 20%, we can see the combination of these two factors that provide acceptable estimations of the AVO-

parameters. When comparing the gas, oil and water scenarios, we observe that the error increases as the impedance contrast decreases.

This information may be useful when designing a seismic survey for monitoring changes of fluids in time-lapse studies. Such methodology can also be utilized for checking the feasibility of applying AVO analysis to old seismic data.

### **ACKNOWLEDGEMENTS**

We thank the sponsors of CREWES for their support. We also acknowledge support from NSERC through the grant CRDPJ 461179-13. Author 1 thanks PEMEX and the government of Mexico for funding his research.

### **REFERENCES**

- Aki, K., and Richards, P., 2002, *Quantitative seismology: theory and methods*: Second Edition, University Science Books, Sausalito, CA.
- Cambois, G., 1998, AVO attributes and noise: pitfalls of crossplotting: In *SEG Expanded Abstracts*, **54**,2,244-247.
- Cordsen, A., Galbraith, M., and Peirce, J., 2000, *Planning land 3-D seismic surveys*: Ed. Tulsa: Society of exploration geophysicists.
- Downton, J. E. and Lines, L. R., 2001, AVO feasibility and reliability analysis: *CSEG recorder*, **26**,6,66-73.
- Galbraith, M., 2004, A new methodology for 3D survey design: *The Leading Edge*, **23**,10, 1017-1023.
- Gassmann, F., 1951. Elastic waves through a packing of spheres: *Geophysics*, **16**, 673-685.
- Russell, B., and Hampson, D., 2006, The old and the new in seismic inversion: *CSEG Recorder*, **31**,10, 5-11.
- Smith, Tad M., Carl H. Sondergeld, and Chandra S. Rai., 2003, "Gassmann fluid substitutions: A tutorial": *Geophysics*, **68**,2, 430-440.